Chapter 9

First-Principles Calculation of Elastic Properties

Michael J. Mehl, Barry M. Klein,* and Dimitris A. Papaconstantopoulos

Complex Systems Theory Branch, Naval Research Laboratory, Washington, DC 20375-5000, USA

1. Introduction

Many first-principles calculations of the electronic structure and total energy of solids have been carried out since the development of high-speed computers (Pickett, 1985). In our group, these calculations have been used to determine equations of state of ionic materials (Feldman *et al.*, 1987, 1988; Mehl *et al.*, 1988) and metals (Sigalas *et al.*, 1990, 1992; Papaconstantopoulos and Singh, 1990; Singh and Papaconstantopoulos, 1990), the pressure at which structural phase transitions occur (Feldman *et al.*, 1988; Mehl *et al.*, 1988), phonon frequencies (Mehl and Pickett, 1989), and new structures (Boyer *et al.*, 1991). The calculations demonstrated the reliability of the technique for predicting ground-state properties of solids.

From the perspective of materials physics, the elastic constants C_{ij} contain some of the more important information that can be obtained from ground-state total-energy calculations. A given crystal structure cannot exist in a stable or metastable phase unless its elastic constants obey certain relationships. The C_{ij} also determine the response of the crystal to external forces, as characterized by the bulk modulus, shear modulus, Young's modulus, and Poisson's ratio, and so play an important part in determining the strength of a material. There is also a tendency toward correlation between the elastic constants and the melting temperature of a solid (Fine *et al.*, 1984; Fleischer, 1991a). Experimentally, the individual C_{ij} can only be determined from single-crystal samples. If only polycrystalline samples are available, then only two independent elastic constants (such as the bulk modulus and isotropic shear modulus) may be measured (Schreiber *et al.*, 1973).

First-principles calculations that use periodic boundary conditions assume the existence of a single crystal; so all elastic constants can be determined by direct computation. The calculated C_{ij} can then be used to check the experimental bulk and shear moduli, if available, and to calibrate model calculations. In addition, the elastic constants can be used to check the phase stability of proposed compounds. For example, it has been shown that B1 (cF8) MoN (Chen *et al.*, 1988), b.c.c. aluminum (Mehl and Boyer, 1991), and b.c.c. iridium (Mehl and Boyer, 1991; Wills *et al.*, 1992) do not exist in Nature because they are elastically unstable. A new metastable phase of Si with fivefold coordination has also been predicted (Boyer *et al.*, 1991). First-principles calculations can thus be used to predict the existence and properties of new materials and phases.

In a theoretical search for new materials, an interesting and important area of research is to study binary compounds that exhibit high melting temperatures and large elastic constants (which roughly correlate with 'strength'). These alloys might be good candidates for new structural materials, were they not brittle. By small ternary additions to these materials, one might hope to improve their ductility while maintaining the high melting temperature and strength. The traditional way to do this is to use quantum structure maps (see Chapter 18 by Pettifor in this volume) to attempt to find appropriate ternary materials for alloying, or brute-force experiments, trying

*Now at: Department of Physics, University of California, Davis, 95616-8677, USA

Intermetallic Compounds: Vol. 1, *Principles*. Edited by J. H. Westbrook and R. L. Fleischer

many possible candidate materials. This may take a long time, as one must search through many materials, using different experimental techniques to properly prepare multiple compounds. In contrast, computer 'experiments' can 'prepare' and analyze the samples quickly. One simply decides where the atoms will sit in the lattice and performs calculations, which will determine whether the initial choice of positions was appropriate. The atoms may then be moved until one finds a mechanically stable system. Of course, the final result of the calculations may be a metastable state that cannot be realized by experiment. Computations and experiments should work hand-in-hand to achieve the goal of fabricating a new alloy.

Even using the largest supercomputers, current first-principles calculations are limited to approximately 100 atoms per unit cell because of computer speed and memory limitations. This can be traced to the fact that the size of the secular equation used in solving the Schrödinger equation by traditional means must be proportional to the number of atoms in the unit cell. For most algorithms currently in use for transition-metal systems, the storage required is proportional to the square of the secular equation set size, while the computational time increases as the cube, quickly limiting the number of atoms that can be treated. Improvements in the performance of scalar or vector computers do not help appreciably, since an order-of-magnitude increase in the speed of a computer would allow only a doubling of the number of atoms that could be handled. Recent advances in numerical techniques indicate that this bottleneck can be removed (Baroni and Giannozzi, 1992; Galli and Parrinello, 1992), but this will require not only new algorithms but also massively parallel computers.

As noted earlier, first-principles calculations can reliably determine a number of basic material properties, including the elastic constants. This provides an estimate of the mechanical stability, strength, and, indirectly, the melting temperature (Fine *et al.*, 1984; Fleischer, 1991a) of alloys that have not been experimentally produced. The calculations also aid in the development of computationally tractable models, which can be used to study thousands of atoms. For example, some of the RuAl data presented below were used to determine an embedded-atom potential to study defects in the RuAl lattice (Rifkin *et al.*, 1992; Becquart, 1992).

We have computed the elastic constants of many intermetallic alloys (Mehl *et al.*, 1990, 1991; Osburn *et al.*, 1991). In this chapter we will describe the techniques used to do the first-principles calculations, the analysis that leads to the calculation of the elastic constants, and present the results of our calculations. We will also discuss the relationship between the elastic constants and the melting temperature, and finally discuss other possible applications of first-principles calculations to materials physics.

2. Theoretical and Computational Details

2.1 Density-Functional Formalism

Modern first-principles electronic-structure calculations in solids are almost always based on the density-functional theory (DFT) of Hohenberg and Kohn (1964). Their theorem states that, for a given external potential (here the Coulomb potential created by the nuclei in the solid), the total energy of an electronic system is a functional of the density of the electrons in the solid, and that the total energy is variational, i.e. small deviations of the density away from the ground state produce positive-definite changes in the total energy which are proportional to the square of the change in the charge density. Thus, in principle, we can calculate the ground-state energy of a system of electrons by searching through possible electronic densities $n(\mathbf{r})$ until we find some minimum energy E. Kohn and Sham (1965) showed how to reduce this to practice. They assumed that the electron density $n(\mathbf{r})$ could be constructed from single-electron orbitals, all of which were eigenstates of a local potential $v_{KS}(\mathbf{r})$. The total energy of a solid can then be written in the form

$$E[n(\mathbf{r})] = T_0[n(\mathbf{r})] + E_H[n(\mathbf{r})] + U_{ext}[n(\mathbf{r})] + E_{xc}[n(\mathbf{r})] + E_{ion} \quad (1)$$

where

$$n(\mathbf{r}) = \sum_{occ} |\phi_i(\mathbf{r})|^2 \quad (2)$$

is the density of electrons in the solid, the $\phi_i(\mathbf{r})$ are the occupied single-particle states,

$$T_0[n(\mathbf{r})] = -(\hbar^2/2m) \sum_{occ} \int \phi_i^*(\mathbf{r}) \nabla^2 \phi_i(\mathbf{r}) \, d^3r \quad (3)$$

is the kinetic energy of a non-interacting set of electrons of density $n(\mathbf{r})$ in the non-relativistic approximation,

$$E_H[n(\mathbf{r})] = (e^2/2) \int \int n(\mathbf{r}) n(\mathbf{r}') / |\mathbf{r} - \mathbf{r}'| \, d^3r \, d^3r' \quad (4)$$

is the Hartree interaction, or the self-Coulomb interaction of the electron density,

$$U_{ext}[n(\mathbf{r})] = -e \int n(\mathbf{r}) V_{ext}(\mathbf{r}) \, d^3r \quad (5)$$

is the interaction between the electrons and the Coulomb field ($V_{ext}(\mathbf{r})$) of the nuclei, $E_{xc}[n(\mathbf{r})]$ is the exchange–correlation energy of the electrons, discussed below, and E_{ion} is the Coulomb interaction between the bare nuclei.

The functional $E_{xc}[n(\mathbf{r})]$ appearing in equation (1) has not been exactly determined. It includes the exchange energy, defined as the energy obtained because the single-particle wavefunctions $\phi_i(\mathbf{r})$ obey the Pauli principle; and the correlation energy, which includes the energy that accounts for the fact that the actual solution of the Schrödinger equation in this problem is not a collection of single-particle states, as well as that part of the kinetic energy that is not accounted for by the term $T_0[n(\mathbf{r})]$. The most widely used approximation for E_{xc} is founded on the observation that, if the charge density $n(\mathbf{r})$ is slowly varying, then the local contribution to the exchange–correlation energy should be identical to the contribution from the uniform electron gas of the same density. This leads to the major approximation in our version of the DFT, the *local-density approximation* (LDA), which yields

$$E_{xc}[n(\mathbf{r})] \approx E_{xc}^{LDA}[n(\mathbf{r})] = \int n(\mathbf{r})\epsilon_{xc}[n(\mathbf{r})]\ d^3r \quad (6)$$

where $\epsilon_{xc}[n]$ is the exchange–correlation energy per electron in the uniform electron gas of density n. There are many approximate expressions for ϵ_{xc}. In this paper we use the parametrization of Hedin and Lundqvist (1971). As we shall see *a posteriori*, this is adequate for our purposes. Currently there is, however, no systematic way to improve upon the LDA; and so this is the only uncontrolled approximation in this method.

If we now substitute expressions (2)–(5) into equation (1) and minimize the total energy subject to the constraint that the ϕ_i are orthonormal, we find that the wavefunctions satisfy the Schrödinger-like equation

$$-(\hbar^2/2m)\nabla^2\phi_i(\mathbf{r}) + v_{KS}(\mathbf{r})\phi_i(\mathbf{r}) = \epsilon_i\phi_i(\mathbf{r}) \quad (7)$$

where v_{KS}, the Kohn–Sham potential, is the functional derivative of all of the terms in (1) *except* $T_0[n(\mathbf{r})]$:

$$v_{KS}(\mathbf{r}) = e^2\int n(\mathbf{r}')/|\mathbf{r}-\mathbf{r}'|\ d^3r' + V_{ext}(\mathbf{r}) + v_{xc}(\mathbf{r}) \quad (8)$$

The exchange–correlation potential $v_{xc}(\mathbf{r})$ is the functional derivative of E_{xc} with respect to the density $n(\mathbf{r})$. In the local-density approximation (6), it takes the form

$$v_{xc}(\mathbf{r}) = \epsilon_{xc}[n(\mathbf{r})] + n(\mathbf{r})\epsilon'_{xc}[n(\mathbf{r})] \quad (9)$$

where the prime on the last term denotes the derivative with respect to $n(\mathbf{r})$.

Given the positions and charges of the nuclei in the system, we can solve for the ground-state charge density (the $n(\mathbf{r})$ that minimizes (1)) by making an initial guess for $n(\mathbf{r})$, using (8) and (9) to calculate the Kohn–Sham potential, and then solve the Schrödinger equation (7) subject to the boundary conditions of the problem (see below) to obtain a new charge density (2). In principle, we could use this new charge density to start the cycle over again, but in practice this is numerically unstable, so we must mix the new and old charge densities together. This mixing can be as simple as a linear combination of the old and new charge densities, or as complicated as the use of the Broyden method (Singh *et al.*, 1986; Johnson, 1988), which accelerates convergence. The mixed charge density is used to calculate a new Kohn–Sham potential (8) and the process begins again. After a number of iterations, typically on the order of 10, the input and output charge densities will be essentially equal, the total energy will have converged, and the solution is self-consistent.

It should be emphasized that the DFT provides an exact relationship only between $n(\mathbf{r})$ and the ground-state energy. Thus the use of the Kohn–Sham formalism that we have outlined here, and particularly the LDA, may not accurately describe excited-state properties. In particular, the eigenvalues ϵ_i, which are often interpreted as single-particle excitation energies, yield band gaps for insulators that are smaller than those found by experiment (Pickett and Wang, 1984). In addition, some quantities that can be computed from LDA ground-state properties may be in error. For example, the LDA usually overestimates the cohesive energy of solids. This is thought to occur because the LDA does a poor calculation of the total energy in isolated atoms (Perdew *et al.*, 1992). The Kohn–Sham formalism often fails to describe adequately highly correlated systems such as the Mott insulators (Terakura *et al.*, 1984). These problems tell us that we should be very careful to test the LDA–DFT method on systems with known properties before we attempt to predict properties of new materials. The following sections describe some of these tests and some predictions.

2.2 *The General-Potential Linear Augmented Plane-Wave Method*

Finding solutions of the Schrödinger equation (7) for a given v_{KS} is the major computational problem in determining the ground-state charge density $n(\mathbf{r})$. In one-dimensional and quasi-one-dimensional problems, such

as spherically symmetric atoms, the boundary conditions are easily specified, and equation (7) may be solved by standard numerical methods for determining eigenvalues and eigenstates (Press *et al.*, 1986). In three dimensions this approach is difficult because the boundary conditions are non-trivial. The most widely used approach is to specify a set of basis functions to restrict the region of Hilbert space that must be searched to determine a solution. The basis functions are constructed to reflect the appropriate symmetry and to satisfy the boundary conditions of the problem. We can formally expand the eigenfunctions ϕ_i in terms of the basis functions ψ_j, which need not be orthonormal:

$$\phi_i(\mathbf{r}) = \sum_j a_{ij}\psi_j(\mathbf{r}) \tag{10}$$

Substituting (10) into (7), multiplying both sides by $\psi_k^*(\mathbf{r})$, and integrating over all space, we find that the a_{ij} and ϵ_i form solutions of the generalized eigenvalue problem,

$$\sum_j (H_{kj} - \epsilon_i S_{kj}) a_{ij} = 0 \tag{11}$$

where

$$H_{kj} = \int \psi_k^*(\mathbf{r})[-(\hbar^2/2m)\nabla^2 + v_{KS}(\mathbf{r})]\psi_j(\mathbf{r})\, d^3r \tag{12}$$

is the Hamiltonian matrix and

$$S_{kj} = \int \psi_k^*(\mathbf{r})\psi_j(\mathbf{r})\, d^3r \tag{13}$$

is the overlap matrix. The resulting eigenstates (10) can be made orthonormal in real space. If the basis set $\psi_i(\mathbf{r})$ is complete, the solution of (11) will provide an exact solution for (7). In practice the basis set is truncated at a finite number of wavefunctions, and the states with the lowest eigenvalues are used as an approximate solution of (7). The variational principle assures that adding more linearly independent basis functions to the set will improve the accuracy of the solution, so this is a controlled approximation.

The first step in picking a set of basis functions is to determine the boundary conditions that they must satisfy. In a solid crystal the external potential $V_{ext}(\mathbf{r})$ and the density $n(\mathbf{r})$ have the periodicity of the lattice, so by (8) the Kohn–Sham potential $v_{KS}(\mathbf{r})$ must have the same period. In this case, the eigenfunctions ϕ_i must satisfy Bloch's theorem (Kittel, 1986),

$$\phi_{kj}(\mathbf{r}) = u_{kj}(\mathbf{r})\exp(i\mathbf{k}\cdot\mathbf{r}) \tag{14}$$

where $\mathbf{k}$ is a vector in the first Brillouin zone of the reciprocal lattice, $u_{kj}(\mathbf{r})$ has the periodicity of the lattice, and j represents the remaining quantum numbers, including spin. The eigenfunctions with different values of $\mathbf{k}$ are orthogonal, so that performing a block diagonalization of the Hamiltonian allows us to concentrate on one $\mathbf{k}$ value at a time. The sums in (2) and (3) are then replaced by an integral in $\mathbf{k}$ over the first Brillouin zone and a sum over the remaining quantum numbers. In practice, we approximate the integral by the special $\mathbf{k}$-point method of Monkhorst and Pack (1976), modified to handle the case of strained lattices when we calculate elastic constants (Mehl *et al.*, 1990). Although not variational, the error in this method decreases as the number of special $\mathbf{k}$ points increases, so this is another controlled approximation.

We are now ready to make a choice of basis set. Although many types of basis sets have been tried in DFT calculations, our experience shows that one of the best choices is the linear augmented plane-wave (LAPW) basis developed by Andersen (1975). In this method the basis functions are indexed by $\mathbf{k}+\mathbf{G}$, where $\mathbf{G}$ is a reciprocal lattice vector. We will describe the method as it is implemented by Wei and Krakauer (1985), which forms the basis of the program we now use. Space is divided into two types of regions: (1) non-overlapping spherical muffin tins surrounding each nucleus in the lattice; and (2) the interstitial region, covering all space not spanned by the muffin tins. In region (1) we would expect the wavefunctions to be rapidly varying and almost atomic-like, while in (2) we expect the potential and the wavefunctions to be slowly varying, and so may be approximated by plane waves. Inside the muffin tins, the wavefunctions have the form

$$\Phi_{\mathbf{k}+\mathbf{G}}(\mathbf{r}) = \sum_{lm}[a_{lm\alpha}u_{l\alpha}(\epsilon_{l\alpha}, \xi_{l\alpha}) + b_{lm\alpha}\dot{u}_{l\alpha}(\epsilon_{l\alpha}, \xi_{l\alpha})]\, Y_{lm}(\theta_\alpha, \phi_\alpha) \tag{15}$$
$$\xi_\alpha = \mathbf{r} - \tau_\alpha,\ |\xi_\alpha| < R_\alpha$$

where the muffin tin centered on site α, located at the position τ_α, has radius R_α. In the interstitial region, the basis function has the simple plane-wave form

$$\Phi_{\mathbf{k}+\mathbf{G}}(\mathbf{r}) = \exp[i(\mathbf{k}+\mathbf{G})\cdot\mathbf{r}] \tag{16}$$

The radial wavefunctions $u_{l\alpha}(\epsilon_{l\alpha}, \xi)$ are solutions of the radial part of Schrödinger's equation (7) with angular momentum l at the energy $\epsilon_{l\alpha}$ and with the potential $v_{KS}(\mathbf{r})$ replaced by its spherical average inside the muffin tin. The $u_{l\alpha}$ are normalized to integrate to unity inside the muffin tin. The function $\dot{u}_{l\alpha}(\epsilon_{l\alpha}, \xi)$ is the

derivative of $u_{l\alpha}$ with respect to the energy parameter and evaluated at $\epsilon_{l\alpha}$. The parameters $a_{lm\alpha}$ and $b_{lm\alpha}$ are chosen so that its gradient will be continuous at the muffin-tin boundaries.

The choice of the energy parameters $\epsilon_{l\alpha}$ is crucial to the success of the method. With a proper selection of these parameters, the basis functions mimic the valence eigenstates inside the muffin tins, reducing the number of basis functions required to achieve convergence. The ideal values would be those which minimize the total energy of the system. As this is difficult to determine, in general we place these parameters within the range of eigenenergies of the band under investigation. The exact location is not crucial. For example, in a 1 Ry (13.6 eV) wide s band, we can find all eigenvalues to within an accuracy of 1 mRy with a single energy parameter (Koelling and Arbman, 1975). If the width of the band becomes too large, or if it is necessary to include some of the lower-lying 'core' states in the problem, we can break the calculation into 'windows', with different energy parameters in each window. This is usually successful, but using a different set of basis functions for each window means that eigenstates in different windows will not be orthogonal to one another. A newer approach recognizes that these low-lying states are nearly localized within the muffin tins and adds a set of specially constructed localized orbitals which relax the linearization of the LAPW method and thereby aid in the representation of these states (Singh, 1991).

Now we are almost ready to set up the Hamiltonian H and overlap matrix S. A few technical details remain: First, we represent the potential $v_{KS}(\mathbf{r})$ by a Fourier expansion into plane waves in the interstitial region, and by an expansion in spherical harmonics inside the muffin tin. The charge density $n(\mathbf{r})$ has a similar representation. In both cases we make use of the symmetry of the lattice to reduce the amount of storage needed. In the calculations presented here, we expand the potential to angular momentum $l=4$ inside the muffin tins, and the density to $l=8$. These cutoffs are, of course, controllable. Second, we must specify the number of basis functions Φ we are going to use. Typically, we use all wavefunctions for which $|\mathbf{k}+\mathbf{G}|R_{\min}<RK_{\max}$, where $R_{\min}$ is the smallest muffin-tin radius, and the constant $RK_{\max}$ is chosen so that the basis set includes 50–100 functions for each atom in the unit cell when the lattice is small enough that the muffin tins are touching. Typically, $RK_{\max}$ is in the range 7.5–8.5. For larger lattices we keep the same size muffin tins and $RK_{\max}$, so the number of basis functions will increase. By making $RK_{\max}$ larger, we may increase the number of basis functions, and monitor the convergence of calculated quantities. Note, however, that the computational time taken to solve (11) by traditional methods is proportional to the cube of the number of basis functions. Since the size of the basis set is proportional to $RK^3_{\max}$, the computational time grows as $RK^9_{\max}$. Thus traditional methods of finding the solution of (11) are rather severely limited by the size and speed of the computer. Fortunately the systems presented here can be solved with quite modest matrix sizes (all use less than 300 basis functions). Finally, we add relativistic corrections, including an averaged spin–orbit term, by replacing (7) by the so-called semi-relativistic approximation (Koelling and Harmon, 1977). The neglected part of the spin–orbit interaction is important for materials with large Z, but it should not affect the calculations presented here.

3. Calculation of the Elastic Constants

3.1 The Equation of State and the Bulk Modulus

Now that we have described our method of calculation, all we need do is to specify a lattice, the charges on the nuclei, and a starting charge density. We then solve the equations (1)–(9) self-consistently, stopping when we have found an accurate total energy (1) and charge density (2). If we limit ourselves to simple lattices, such as the NaCl or B1 structure (Pearson symbol cF8) and the CsCl or B2 (cP2) structure, then the internal lattice parameters will be fixed once we specify the volume of the system. We can thus determine a set of total energies $E_i=E(V_i)$. In practice, we use several volumes which are within 10–20% of the expected equilibrium volume. If the minimum is not within this range we extend the range until we have the minimum bracketed. We then make a least-squares fit of the set (V_i,E_i) to a form proposed by Birch (1978):

$$E_{\text{Birch}}=E_0+\tfrac{9}{8}B_0V_0[(V_0/V)^{2/3}-1]^2+\tfrac{9}{16}B_0V_0(B_0'-4)\times[(V_0/V)^{2/3}-1]^3+\sum_{n=4}^{N}\gamma_n[(V_0/V)^{2/3}-1]^n \quad (17)$$

where E_0, V_0, B_0, and B_0' are, respectively, the equilibrium energy, volume, bulk modulus, and pressure derivative of the bulk modulus, while N is the order of the fit. For a second-order fit, it is obvious that $B_0'=4$. In most cases we find that B_0' is between 3 and 5. The choice of the Birch cutoff N is rather important. If we have only $N+1$ pairs (V_i,E_i) then equation (17) will exactly track the input, $E_B(V_i)=E_i$. Unfortunately, there will be numerical errors in the calculation of E_i,

caused by such things as the change in basis set with changing lattice constant and errors in the Brillouin-zone integrations. This noise might cause $E_B(V)$ to oscillate in the region of the equilibrium, and so the bulk modulus, which is computed from

$$B_{\text{Birch}}(V) = VE''_{\text{Birch}}(V) \tag{18}$$

may oscillate rapidly and unphysically. We must therefore truncate N at some value less than the total number of points in the calculation. The method we use to determine the value of N is outlined in the appendix (Section 7.1). In most of the computations presented here we found $N=3$ to be adequate.

In this chapter we consider two classes of lattices. The first is cubic and contains the monatomic b.c.c. and f.c.c. lattices as well as the diatomic B1 (cF8), B2 (cP2), and $L1_2$ (cP4) structures. The second is the tetragonal $L1_0$ (tP4) structure. The cubic structures are completely specified by one parameter, the volume of the unit cell V, or alternatively the cube side a.

The only member of the second class we study here is the $L1_0$ (tP4) lattice, which is completely specified by two lattice parameters. In the traditional representation of this lattice, the two lattice parameters are a and c (see Figure 1), and the primitive vectors are

$$\begin{aligned} \mathbf{a}_1 &= (a/2,\ -a/2,\ 0) \\ \mathbf{a}_2 &= (a/2,\ a/2,\ 0) \\ \mathbf{a}_3 &= (0,\ 0,\ c) \end{aligned} \tag{19}$$

There are two atoms in the basis, located at the points

$$\begin{aligned} \mathbf{b}_1 &= (0,\ 0,\ 0) \\ \mathbf{b}_2 &= (a/2,\ 0,\ c/2) \end{aligned} \tag{20}$$

If $c=a/\sqrt{2}$, then the $L1_0$ lattice reduces to the B2 structure, while if both atom types are identical and $c=a$, it becomes an f.c.c. lattice.

When dealing with the tetragonal lattice we must specify what we mean by $E_i=E(V_i)$, the energy of the lattice at the volume V_i. If we let $E(a,c)$ denote the energy of the lattice (19)–(20), and fix $a^2c/2=V_i$, then $E(V_i)$ is the minimum of all of the $E(a,c)$ at this volume. To approximate E_i, at each V_i we choose five different c/a ratios, which we will denote by the symbol ζ, around $c/a=1$. We fit the total energy $R(V_i, \zeta)$ to a third-order polynomial in ζ. The minimum of energy of this polynomial is assumed to be E_i, and the associated c/a ratio is called ζ_i. We can then specify the volume behavior of the energy by fitting the pairs (V_i,E_i) to the Birch form (17), and the volume behavior of the c/a ratio by fitting the pairs (V_i, ζ_i) to the Birch-like form

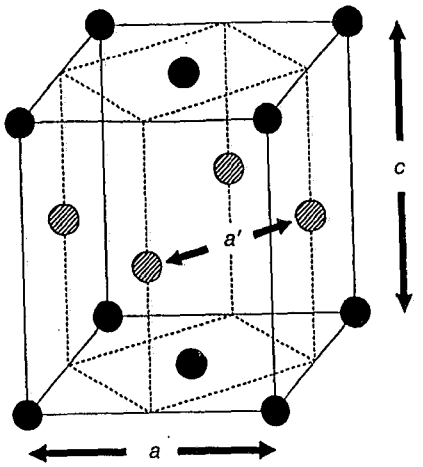

Figure 1. The $L1_0$ (tP4) structure of NbIr and TiAl. This is an f.c.c.-based structure where the two types of atoms alternate in [001] planes. The distances a and c describe the lattice in terms of the vectors (19), while the distances a' and c define the lattice in terms of the primitive vectors (32). The broken lines show the position of the primitive unit cell, which contains one atom of each type

$$\zeta(V) = \sum_{n=0}^{N} z_n V^{-2n/3} \tag{21}$$

The function $\zeta(V)$ then represents the c/a ratio that minimizes the total energy at the volume V.

3.2 Calculation of the Remaining Elastic Constants

If we strain the lattice by distorting the primitive vectors and relax all of the internal parameters to minimize the total energy (1), we may obtain all of the elastic constants C_{ij} (Ashcroft and Mermin, 1976). Define a strain tensor $\overleftrightarrow{\epsilon}$, such that the primitive vectors $\mathbf{a}_i$ are transformed to the new vectors

$$\begin{pmatrix} \mathbf{a}'_1 \\ \mathbf{a}'_2 \\ \mathbf{a}'_3 \end{pmatrix} = \begin{pmatrix} \mathbf{a}_1 \\ \mathbf{a}_2 \\ \mathbf{a}_3 \end{pmatrix} \cdot (\overleftrightarrow{1} + \overleftrightarrow{\epsilon}) \tag{22}$$

where $\overleftrightarrow{1}$ is the 3×3 identity matrix. We need only consider non-rotating strains, so we represent the strain by a symmetric tensor with six independent components:

$$\overleftrightarrow{\epsilon} = \begin{pmatrix} e_1 & e_6/2 & e_5/2 \\ e_6/2 & e_2 & e_4/2 \\ e_5/2 & e_4/2 & e_3 \end{pmatrix} \tag{23}$$

Then the total energy changes by an amount

$$E(e_i)=E_0-P(V)\Delta V+V\sum_{i=1}^{6}\sum_{j=1}^{6}C_{ij}e_ie_j/2+O[e_i^3] \tag{24}$$

where V is the volume of the undistorted lattice, $P(V)$ is the pressure of the undistorted lattice at volume V, ΔV is the change in the volume of the lattice due to the strain (23), and $O[e_i^3]$ indicates that the neglected terms in the polynomial expansion are cubic and higher powers of the e_i.

There are 21 independent elastic constants C_{ij} in (24). Symmetry reduces this number to three for the cubic lattices, and six for the tetragonal $L1_0$ lattice. At any volume V, the bulk modulus B (18) can be related to these constants by the formula

$$B=(C_{11}+2C_{12})/3 \tag{25}$$

for cubic lattices and

$$B=[(C_{11}+C_{12})C_{33}-2C_{13}^2]/(C_{11}+C_{12}+2C_{33}-4C_{13}) \tag{26}$$

for any tetragonal lattice, in particular the $L1_0$ lattice.

The remaining constants must be calculated by other means. For cubic lattices, we need two more constants to complete the set. The logical choices are the shear modulus $(C_{11}-C_{12})/2$ and the modulus C_{44}. These are the physically important combinations, since a cubic material will not be mechanically stable (to $O[x^2]$) unless

$$B=(C_{11}+2C_{12})/3>0, \qquad C_{11}-C_{12}>0 \qquad C_{44}>0 \tag{27}$$

at the equilibrium of the equation of state.

Although the obvious method of computing $C_{11}-C_{12}$ uses the tetragonal strain (Mehl *et al.*, 1990), we now prefer the volume-conserving orthorhombic strain,

$$e_1=-e_2=x \qquad e_3=x^2/(1-x^2) \qquad e_4=e_5=e_6=0 \tag{28}$$

This has the advantage that the energy is an even function in the strain x, changing by an amount

$$\Delta E(x)=\Delta E(-x)=V(C_{11}-C_{12})x^2+O[x^4] \tag{29}$$

and we need only half as many computations as are required using the tetragonal symmetry. Although the orthorhombic strain has lower symmetry and thus needs more independent **k** points for Brillouin-zone averages than the tetragonal strain, we prefer this method because of the reduction in the number of self-consistent calculations needed.

We perform a similar trick for the C_{44} modulus, where we use a volume-conserving monoclinic strain,

$$e_6=x \qquad e_3=x^2/(4-x^2) \qquad e_1=e_2=e_4=e_5=0 \tag{30}$$

Again the total energy is an even function of the strain x:

$$\Delta E(x)=\Delta E(-x)=VC_{44}x^2/2+O[x^4] \tag{31}$$

The tetragonal $L1_0$ (tP4) lattice has six independent constants. As noted above, the bulk modulus is related to these constants via (26). In principle it would be possible to find five independent strains and to use these and the bulk modulus to determine the constants. In practice, we used six independent strains, listed in Table 1, to calculate all six of the constants, and checked our results by comparing the two sides of (26). Notice that the first three strains in Table 1, while not volume-conserving, all have the symmetry of the $L1_0$ lattice and so can be calculated from our original data $E(V,\zeta)$ (or $E(a,c)$). These are also the only constants needed to compute the bulk modulus (26). The remaining strains conserve the volume but no longer have full tetragonal symmetry. In these cases we chose the strains so that the energy was an even function of the strain.

The choice (19)–(20) to represent the $L1_0$ structure is not unique. This selection corresponds to taking an f.c.c. lattice and stacking (001) planes of atom type B upon (001) planes of atom type A, then letting the lattice parameters a and c relax to minimize the energy.

Table 1. Strains and energy changes for the tetragonal $L1_0$ (tP4) phase. Unlisted e_i are set to zero

Strain	Parameters	$\Delta E/V$
1	$e_1=e_2=x$	$(C_{11}+C_{12})x^2+O[x^3]$
2	$e_1=e_2=x$ $e_3=-x(2+x)/(1+x)^2$	$(C_{11}+C_{12}+2C_{13}-4C_{13})x^2+O[x^3]$
3	$e_3=x$	$C_{33}x^2/2+O[x^3]$
4	$e_1=[(1+x)/(1-x)]^{1/2}-1$ $e_2=[(1-x)/(1+x)]^{1/2}-1$	$(C_{11}-C_{12})x^2+O[x^4]$
5	$e_4=e_5=x$ $e_3=x^2/4$	$C_{44}x^2+O[x^4]$
6	$e_6=x$ $e_1=e_2=(1+x^2/4)^{1/2}-1$	$C_{66}x^2/2+O[x^4]$

An alternative view considers the $L1_0$ structure as a body-centered tetragonal lattice (see Figure 1). In this case the primitive vectors take the form

$$\begin{aligned} \mathbf{a}_1' &= (a', 0, 0) \\ \mathbf{a}_2' &= (0, a', 0) \\ \mathbf{a}_3' &= (0, 0, c) \end{aligned} \tag{32}$$

with basis vectors

$$\begin{aligned} \mathbf{b}_1' &= (0, 0, 0) \\ \mathbf{b}_2' &= (a'/2, a'/2, c/2) \end{aligned} \tag{33}$$

where $a' = a/\sqrt{2}$. Note that both (19)–(20) and (32)–(33) describe the same unit cell, indicated by the broken lines in Figure 1. The later representation can be obtained from the former by a 45° rotation about the z-axis. Since the C_{ij} are actually components of a fourth-order tensor, the components in the old (unprimed) and new (primed) frames are related by the linear transformations:

$$\begin{aligned} C_{11}' + C_{12}' &= C_{11} + C_{12} & C_{11}' - C_{12}' &= 2C_{66} \\ C_{66}' &= (C_{11} - C_{12})/2 & C_{13}' &= C_{13} \\ C_{33}' &= C_{33} & C_{44}' &= C_{44} \end{aligned} \tag{34}$$

We will present our results in both coordinate systems. Note that the bulk modulus (26) is independent of the choice of coordinate system.

Once the elastic constants are determined, we would like to compare our results with experiment, or predict what an experiment would yield for the elastic constants. A problem arises when single-crystal samples cannot be obtained, for then it is not possible to measure the individual elastic constants C_{ij}. Instead, the isotropic bulk modulus B and shear modulus G are determined. These quantities cannot in general be calculated directly from the C_{ij}, but we can use our values to place bounds on the isotropic moduli. Reuss (1929) found lower bounds for all lattices, while Voigt (1928) discovered upper bounds. For the specific case of cubic lattices, Hashin and Shtrikman (1962) found stricter bounds. We will list the formulas for these bounds in the appendix (Section 7.2). For now, we merely note that the width of the bounds on the shear modulus is related to the anisotropy constant

$$A = 2C_{44}/(C_{11} - C_{12}) \tag{35}$$

As A approaches unity, the crystal becomes isotropic, and the gap between the bounds vanishes.

We also list some auxiliary quantities that are often quoted in the literature. The Young's modulus for an isotropic solid is related to B and G by the formula (Schreiber *et al.*, 1973)

$$E = 9BG/(3B + G) \tag{36}$$

Poisson's ratio is also of interest:

$$\nu = (3B - E)/(6B) \tag{37}$$

Now that we have the formalism, it remains to calculate the moduli. We begin by selecting the elastic modulus to study and then compute the total energy E_i as a function of the strain x_i. Generally we obtain five or six points (x_i, E_i), including the origin, and take x ranging between 0 and 0.1. In the general case, when we strain the primitive vectors by (22) we must adjust the basis vectors to minimize the total energy. However, in the case of every lattice type discussed here, all of the atoms are at inversion sites in the high-symmetry structure. The inversion sites still exist when the lattice is strained according to (22), and we assume that these inversion sites remain stable under strain, i.e. the potential seen by each atom has a local minimum at the inversion site. This is certainly the case for small strains. At larger strains the inversion site may become a saddle point or a local maximum, but this will not affect the behavior for small strains, or our taking the limit as the strain $x \to 0$.

Once we have the strain, given by (28), (30), or one of the formulas in Table 1, we can compute the corresponding linear combination of the C_{ij} by fitting the data pairs (x_i, E_k) to a polynomial in x using the least-squares fit outlined above. For most of the strains outlined here, the odd powers of x vanish identically because $\Delta E(-x) = \Delta E(x)$. For the other cases (the first three strains listed in Table 1) we can eliminate the odd powers of x by defining an average energy,

$$\bar{E}(x) = \bar{E}(-x) = [E(x) + E(-x)]/2 \tag{38}$$

Then all energies may be fitted to a polynomial in x^2, eliminating the possibility of numerical noise driving the minimum of the fit away from $x = 0$. The order of this polynomial is selected in the same manner as the order of the Birch fit for the $E(V)$ curve, by choosing the order N that gives the largest value of q (appendix, Section 7.1). The coefficient of the x^2 term is proportional to the elastic constant times the volume of the system, and we can estimate the error in the modulus using the technique outlined in the appendix.

4. Results

4.1 Monatomic Systems

We begin by testing our method on several simple monatomic metals. Our first calculations will be to determine the equation of state and equilibrium parameters, V_0, B_0, and B_0', and to compare the results with experiment. The simple metals we choose include three f.c.c. materials, Ca, Al, and Ir, and b.c.c. Mo. We also look at two phases of Li, the b.c.c. phase, observed at room temperature, and the f.c.c phase, which is sometimes observed as Li is cooled toward its ground-state h.c.p. phase (Donohue, 1974). The resulting equilibrium parameters are shown in Table 2, along with the experimental room-temperature lattice constants (Donohue, 1974), and low-temperature bulk moduli where available (Simmons and Wang, 1971). We will compare the bulk modulus with experiment when we discuss the elastic constants. In all cases we find that the experimental lattice constant is larger than the predicted a_0. In part this is due to thermal expansion and zero-point motion (see below), which are not considered in our calculations, but the major part of the error is due to the LDA. In particular, the large error for calcium is typical of errors made using the LDA for alkali and alkaline earth metals (Sigalas *et al.*, 1992; Perdew *et al.*, 1992). The errors for the other materials are also typical of other LDA calculations (Moruzzi *et al.*, 1978). For example, a set of calculations of the total energy and bulk modulus for all 3d, 4d, and 5d elements in both the f.c.c. and b.c.c. structures is given by Sigalas *et al.* (1992). These calculations give the correct energy ordering between f.c.c. and b.c.c. across the periodic table, except for iron, where the magnetic structure is not treated correctly by the LDA (Moroni, 1992).

We next calculated the elastic constants of these materials, using the strain (28) to determine $C_{11}-C_{12}$ and the strain (30) to find C_{44}. The number of k points used in these calculations varied with the choice of materials. For Li and Al, where the energy changes $\Delta E(x)$ are small, we were forced to use many k points (up to 7000 k points in the irreducible orthorhombic and monoclinic cells) to reduce the numerical noise in the calculations so that we could reliably extract the elastic constants. For Mo, which has large C_{ij}, we used up to 400 k points in the irreducible part of the Brillouin zone, and we probably could have used fewer points. The calculations described here, however, need relatively few basis functions for convergence (approximately 100 for Mo, 50 for Al and Li) and so may be run quickly on a deskside workstation even with a larger number of k points. In general, a large number of basis functions is needed for transition metals such as Mo because the valence states have major d components, which tend to be localized around the nucleus.

Since experimental data are usually presented at room temperature and pressure, we calculated the elastic constants of the cubic materials at the experimental lattice constants. There are two sources of error in the calculation. The first is the error caused by our neglect of thermal and zero-point vibration. This has been studied by Moruzzi *et al.* (1988). Their method uses a Debye model to approximate the phonon spectra of monatomic cubic metals. Comparing their predicted room-temperature bulk modulus with the static bulk modulus evaluated at the same volume, we find that the vibrational contribution changes the bulk modulus by less than 2 GPa in Li, Al, and Mo. This is on the order of the error in our estimates of the elastic constants and so can safely be neglected.

The second, and possibly serious, error is the inaccuracy caused by the LDA. As seen in Table 2, the LDA underestimates the equilibrium lattice constants. Only part of this error can be attributed to thermal and zero-point motion. For example, Moruzzi *et al.* (1988) found that vibrational motion increased the equilibrium lattice constant by 0.5% over the static lattice constant,

Table 2. Calculated LDA equation-of-state parameters for some simple monatomic metals

		Theory			Experiment		
Element	Structure	a_0 (Å)	B_0 (GPa)	B_0'	a (Å)[a]	B_0 (GPa)[b]	B_0'[b]
Li	f.c.c.	4.28	15.0±0.1	3.4±0.2	4.39		
Li	b.c.c.	3.36	15.1±0.2	3.1±0.5	3.48	13.3 (78 K)	
Ca	f.c.c.	5.34	19	3.4	5.5882		
Al	f.c.c.	3.99	82±1	4.3	4.04953	79 (0 K)	4.42
Mo	b.c.c.	3.12	291±5	4	3.15	265 (0 K)	
Ir	f.c.c.	3.82	402	4.7	3.8391		

[a]Room-temperature experimental lattice constants from Donohue (1974).
[b]Low-temperature experimental moduli from Simmons and Wang (1971).

compared to the 0.4% increase in the experimental lattice constant from absolute zero (but including zero-point motion) to room temperature (Simmons and Wang, 1971). Applying this 0.5% increase to our Al calculations, we predict a room-temperature equilibrium lattice constant of 4.01 Å, which is still substantially smaller than the experimental value of 4.05 Å. Thus our LDA calculations will not be in equilibrium at the experimental room-temperature lattice constant even if we were to include thermal and zero-point vibration in our calculations. The errors introduced by this approximation can be reduced with the use of improved density functionals (Perdew *et al.*, 1992). The good agreement we obtain with experiment may be regarded as an empirical demonstration that the resulting error in the C_{ij} is not serious.

We present our results for the elastic constants in Table 3. For comparison, the static lattice results for Al and b.c.c. Li are also included. Where available, we also present the experimental measurements (Simmons and Wang, 1971; Featherstone and Neighbors, 1963). The results are quite encouraging. Of the elements for which there are experimental values of the elastic constants, the largest error (22%) is in the calculated C_{44} of molybdenum. The error in C_{12} of aluminum is 18%, but the error in the actual computed and measured quantities, B and $C_{11}-C_{12}$, are 12% and 9%, respectively. All other constants are within 11% of the experimental numbers. This indicates that the errors in the LDA do not significantly alter the curvature of the potential surface in most of these compounds. In fact, we might conclude that all of these effects are linear in the volume over the small volume range from the LDA equilibrium volume to the experimental volume, and so have negligible effect on the C_{ij}, which are second order in the strain.

Table 3. Experimental and calculated elastic constants for some cubic monatomic metals

Element	Structure	a_0(Å)	C_{11} (GPa)	C_{12} (GPa)	C_{44} (GPa)
Li	f.c.c.	4.39	14.1±0.5	7.8±0.3	8.6±0.5
Li	b.c.c.	3.36	15.6±0.3	14.8±0.3	11.2±0.2
		3.48	11.4±0.3	10.2±0.2	10±1
	(Exp.)[a]		13.5	11.4	8.8
Ca	f.c.c.	5.59	16.7±0.8	9.7±1	14.2±0.2
Al	f.c.c.	3.99	121±2	63±1	33±5
		4.05	100±3	50±2	31±1
	(Exp.)[a]		107	61	28
Mo	b.c.c.	3.15	468±10	149±6	98±9
	(Exp.)[b]		450	172.9	125
Ir	f.c.c.	3.84	621±7	256±6	260±5
	(Exp.)[a]		590	249	262

[a]Experimental data from Simmons and Wang (1971).
[b]Experimental data from Featherstone and Neighbors (1963).

One consequence of our use of the experimental equilibrium volume to calculate the elastic constants is that the bulk modulus calculated from Table 3 will not in general be equal to the bulk modulus in Table 2. For example, in Table 2 the bulk modulus of Mo is given as 291 GPa, while calculating B from Table 3 yields 255 GPa. The difference reflects the change in bulk modulus with volume. This change is characterized by B_0', the pressure derivative of the bulk modulus at equilibrium. In most cases B_0' is between 3 and 5, with $B_0'=4$ for the second-order Birch fit (17). Thus a 10 GPa change in pressure will change the bulk modulus by about 40 GPa. Both theorists and experimentalists should be very careful to specify the conditions under which the bulk modulus was computed or measured.

4.2 Ordered Binary Intermetallics

We began our work in this area with the explicit goal of using first-principles methods to calculate the elastic constants of ordered binary intermetallic alloys. As mentioned in the introduction, we are particularly interested in those alloys which exhibited high melting temperatures. For this reason our calculations are not a systematic study of all possible binary alloy systems (although there is a large amount of work on aluminum alloy systems).

We begin with the ordered cubic intermetallics with composition A_xB_y, and with all atoms sitting on inversion sites. For the present we have limited our calculations to the B1 (cF8), B2 (cP2), and $L1_2$ (cP4) structures. Since all atoms sit on inversion sites, there is no requirement to relax the internal parameters as we strain the crystal. Again, the calculations were performed at the experimental lattice constant.

The equilibrium equation-of-state parameters for the cubic binary intermetallics are shown in Table 4, and the calculated elastic constants are shown in Table 5. The equilibrium lattice constants are 0.6–3% smaller

Table 4. Calculated LDA equation-of-state parameters for several ordered cubic intermetallic alloys

Compound	Structure	a_0 (Å)	B_0 (GPa)	B_0'	a_{exp} (Å)
FeAl	B2 (cP2)	2.82	195	4	2.91[a]
CoAl	B2 (cP2)	2.80	207±2	4.4±0.3	2.8619[a]
NiAl	B2 (cP2)	2.84	186±7	4.2±0.5	2.8864[a]
Ni_3Al	$L1_2$ (cP4)	3.49	229±2	4.4±0.7	3.58[a]
RuAl	B2 (cP2)	2.96	230±3	4.5±0.2	2.99[b]
RuZr	B2 (cP2)	3.22	228±3	3.6±0.1	3.253[a]
SbY	B1 (cF8)	6.12	65±3	4	6.155[a]

[a]Experimental lattice constant from Pearson (1967).
[b]Experimental lattice constant from Fleischer (1993b).

Table 5. Calculated and experimental LDA elastic constants for several ordered intermetallic alloys. In most cases the experimental room temperature lattice constants are used. NiAl and RuAl have two lattice constants listed, as explained in the text. Note the large variation in the C_{ij} with lattice constant for these stiff materials

Compound	Structure	a_0 (Å)	C_{11} (GPa)	C_{12} (GPa)	C_{44} (GPa)
FeAl	B2 (cP2)	2.94	182±1	78±1	45±7
CoAl	B2 (cP2)	2.86	251±4	101±3	134±1
NiAl	B2 (cP2)	2.84	237±10	155±8	132±5
		2.89	193±5	124±4	114±8
(Exp.)[a]		2.89	211.5	143.2	112.1
Ni_3Al	$L1_2$ (cP4)	3.58	227±5	148±5	120±2
(Exp.)[b]		3.58	220.1	146.0	123.6
RuAl	B2 (cP2)	2.99	308±6	144±5	122±10
		3.03	258±2	118±1	125±1
RuZr	B2 (cP2)	3.22	375±3	154±2	78±1
SbY	B1 (cF8)	6.11	175±11	14±11	23±1

[a]Experimental data from Simmons and Wang (1971).
[b]Experimental data from Wallow *et al.* (1987).

Table 6. Computed LDA equilibrium lattice constants for the $L1_0$ compounds. Experimental data are from Pearson (1967)

	a (Å)		*c* (Å)		*c/a*	
Compound	Theory	Experiment	Theory	Experiment	Theory	Experiment
TiAl	3.90	4.005	4.05	4.070	1.037	1.016
NbIr	3.99	4.027	3.86	3.863	0.967	0.958

than experiment (Pearson, 1967), as is typical of the LDA. To show the variation of elastic constants with *a*, we show the LDA equilibrium elastic constants for NiAl as well as the constants evaluated at the experimental value. The increase in volume decreases the elastic constants by 15–25%. At present, we have performed calculations on only two systems where all of the C_{ij} have been measured experimentally, B2 NiAl (Simmons and Wang, 1971) and $L1_2$ Ni_3Al (Wallow *et al.*, 1987). The modulus with the worst relative error is C_{12} in NiAl, which has an error of 14%. The error in NiAl's C_{11} is 9%, and all other constants are closer to experiment. The polycrystalline bulk and shear moduli have been measured for other systems, so we will be able to make other comparisons with experiment when we calculate the shear modulus in Section 4.3 below.

Table 5 lists two sets of values for the elastic constants of RuAl. Our original calculations (Mehl *et al.*, 1991) assumed the lattice constant of 3.03 Å listed in Pearson (1967). However, recent experimental work by Fleischer (1993b) indicates that the correct lattice constant is 2.99 Å. We present calculated elastic constants for both lattice dimensions.

We next discuss two tetragonal systems with $L1_0$ (tP4) symmetry, TiAl and NbIr. TiAl was actually one of the first binary intermetallics to have its constants calculated (Chubb *et al.*, 1988). As we noted above, there are six independent elastic constants C_{ij} in these systems. Since some of these are calculated via volume-changing strains (the first three in Table 1), we calculated the C_{ij} at the LDA equilibrium to avoid the appearance of the pressure term in (24). Table 6 lists the equilibrium lattice constants predicted by the theory and compares them with experiment. The theoretical value of *c* seems to be closer to experiment than *a*, so the *c/a* ratio is overestimated by 1–2% while the equilibrium volume is underestimated by about 2–6%, a value similar to the above calculations for cubic systems. Table 7 gives the elastic constants for both systems, in both the frame of primitive vectors (19) (unprimed) and the alternative

Table 7. LDA equilibrium elastic constants for the $L1_0$ compounds

Compound	Modulus	Unprimed frame lattice (19) (GPa)	Primed frame lattice (32) (GPa)
TiAl	C_{11}	188±5	243±10
	C_{12}	98±5	43±10
	C_{13}	96±9	96±9
	C_{33}	190±10	190±10
	C_{44}	126±2	126±2
	C_{66}	100±5	45±3
NbIr	C_{11}	430±20	580±20
	C_{12}	270±20	120±20
	C_{13}	250±20	250±20
	C_{33}	490±20	490±20
	C_{44}	175±5	175±5
	C_{66}	230±10	80±10

b.c.t. vectors (32) (primed). Single crystals of these compounds have yet to be grown. Although we cannot compare our C_{ij} to experiment, in the next section we will be able to compare the isotropic bulk and shear moduli to measurements.

4.3 Predictions for Polycrystalline Phases

As mentioned earlier, many of the intermetallic alloys are not available as single crystals, but the isotropic bulk and shear moduli can be measured from polycrystalline samples. We use our elastic constants to predict bounds on these moduli as outlined in the appendix (Section 7.2). We can also calculate the expected Young's modulus (36) and Poisson's ratio (37) for these materials. Table 8 presents these results, including the experimental measurements, when they are available (Featherstone and Neighbors, 1963; Gilmore, 1968; Simmons and Wang, 1971; Fleischer *et al.*, 1989; Fleischer, 1991b, 1993a). We also list the anisotropy factor A (35). For the cases where Table 5 lists the C_{ij} at two different lattice constants (NiAl and RuAl), we use the data from the experimental lattice constant. For the cubic materials we take the average of the Hashin and Shtrikman bounds (appendix, Section 7.2). The difference between the two bounds is on the order of the errors in the inidividual C_{ij} shown in Tables 3 and 5, reaching a maximum of 3.5 GPa in SbY, so the error in G will be on the order of the error in the C_{ij}. For the tetragonal materials TiAl and NbIr we take the average of the Voigt and Reuss bounds. In this case the difference between the two values of G is rather large, so we quote the error as one-half the difference between the bounds.

In comparing experiment and theory, we note that we do very well in predicting the bulk moduli and shear modulus. Of particular note is the value of G for CoAl, which was predicted before we obtained the experimental data (Fleischer, 1993a). Also of interest are the predictions for RuAl. Using our old calculations at the experimental volume listed in Pearson (1967), we found $B=165$ GPa, $G=99$ GPa, $E=248$ GPa, and $\nu=0.25$. The predicted bulk modulus is then 20% smaller than the experimental value. However, when we use the correct lattice constant of 2.99 Å (Fleischer, 1993b), we find that the predicted bulk modulus is only 4% smaller than experiment.

The major discrepancies between theory and experiment in Table 8 are the bulk modulus of Ca (40% error, but an error of only 8 GPa) and the shear modulus for NbIr (16–75% error, dependng on the location of G within the Reuss–Voigt bounds). The errors in B and G for NbIr would decrease if we expand the lattice from the LDA equilibrium lattice parameters to the experimental parameters. All other calculations are within 12% of experiment.

4.4 Predictions of Melting Temperature

As we remarked earlier, Fine *et al.* (1984) showed that there is a rough correlation between the average elastic

Table 8. Predicted isotropic moduli and anisotropy constants. All calculations are at the experimental volume except TiAl and NbIr, which are evaluated at the LDA equilibrium volume. The moduli B, G and E are in GPa

	Theory					Experiment				
Material	B	G	E	ν	A	B	G	E	ν	A
Li (f.c.c.)	9.9	5.8	14	0.35	2.7					
Li (b.c.c.)[a]	10.6	3.4	9.3	0.40	16.7	12.1	3.9	10.5	0.36	8.38
Ca[b]	12	8.1	20	0.22	4.1	20	8.9	23.3	0.30	
Al[a]	67	28	75	0.31	1.24	76	26	70	0.35	1.22
Mo[c]	255	119	310	0.30	0.61	265	130	336	0.29	0.90
Ir[a]	378	226	564	0.25	1.42	363	221	550	0.25	1.54
FeAl	113	48	126	0.31	0.87					
CoAl[d]	151	106	258	0.21	1.78	162	114	277	0.22	
NiAl[e]	147	71	184	0.29	3.29	166	70	184	0.31	3.28
Ni_3Al[e]	174	77	202	0.31	3.04	171	79	205	0.30	3.49
RuAl[f]	199	104	266	0.28	1.49	208	106	271	0.28	
RuZr	228	90	237	0.33	0.70					
SbY[g]	68	38	96	0.26	0.28	66	40.5	101	0.25	
TiAl	127 ± 7	80 ± 10	198	0.24						
NbIr[g]	320 ± 30	145 ± 30	378	0.30		301	99.3	268	0.35	

Experimental data from:
[a]Simmons and Wang (1971).
[b]Gilmore (1968).
[c]Featherstone and Neighbors (1963).
[d]Fleischer (1993a).
[e]Wallow *et al.* (1987).
[f]Fleischer *et al.* (1991b).
[g]Fleischer *et al.* (1989).

constant $(C_{11}+C_{22}+C_{33})/3$ and the melting temperature. Fleischer (1991a) found a similar relationship between T_m and G. For cubic metals Fine *et al.* find

$$T_m = [553\,\text{K} + (5.91\,\text{K/GPa})C_{11}] \pm 300\,\text{K} \quad (39)$$

while for tetragonal materials

$$T_m = [254\,\text{K} + (4.50\,\text{K/GPa})(2C_{11}+C_{33})/3] \pm 300\,\text{K} \quad (40)$$

In Table 9 we show the predicted melting temperatures for these systems and compare them with experiment (Ashcroft and Mermin, 1976; Massalski *et al.*, 1986). While the predictions are reasonably accurate for many materials, the high-melting-temperature materials such as Mo, Ir, and NbIr fall well outside of the 300 K error bars of the prediction. However, the rough correlation between C_{11} and T_m still holds. The substance with the largest error, however, is SbY, which simply has elastic constants too small to be consistent with the measured high melting temperature. This is also substantiated by Fleischer (1991a), who found a correlation between T_m and the shear modulus G. The measured value of G in SbY is also low compared to its melting temperature.

A recent paper (Willis *et al.*, 1992) studying the monatomic transition metals noted that, when one changes a lattice from f.c.c. to b.c.c. by use of a large tetragonal shear, the elastic constant $C_{11}-C_{12}$ was related to the difference in energy between the f.c.c. and b.c.c. phases. This work is reminiscent of the work of Boyer and others (Boyer *et al.*, 1991; Mehl and Boyer, 1991) on 'magic strains' (Boyer, 1989; Van de Waal, 1990). Mehl and Boyer (1991) showed that the 'magic strain' barrier in an f.c.c. material was related to the energy as a function of the tetragonal shear, the 'Bain's path' mentioned by Wills *et al.* (1992). It was also speculated that it is the height of this barrier that determines the melting temperature, not any linear combination of elastic constants. We may speculate on a resolution of the problem of SbY as follows: As there is no simple b.c.c.-based structure for SbY that can be reached by a tetragonal shear, consider a strain along the [1 1 1] axis that will transform B1 SbY into B2 SbY. It is possible that it is the barrier height in this direction, which is related to C_{44}, that controls the melting temperature in SbY. Note that Table 5 shows that C_{44} in SbY is much smaller than it is for the other high-melting-temperature alloys, so the answer is not a simple one. If the correlation between the 'magic strain' barrier height and the melting temperature is to hold in this case, there must be an anomalous relationship between the elastic constants and the barrier height.

Table 9. Predicted melting temperatures

Material	T_m (K) Theory	Experiment
Li (b.c.c.)	620	454[a]
Ca	650	1124[a]
Al	1150	933[a]
Mo	3320	2890[a]
Ir	4230	2683[a]
FeAl	1630	1583[b]
CoAl	2040	1921[b]
NiAl	1700	1911[b]
Ni_3Al	1890	1668[b]
RuAl	2380	2193[b]
RuZr	2770	2373[b]
SbY	1590	2583[b]
TiAl	1370	1746[b]
NbIr	2830	2113[b]

[a]Experimental data from Kittel (1986).
[b]Experimental data from Massalski *et al.* (1986).

5. Summary

We have shown that it is possible to use the formalism of density-functional theory and the local-density approximation to calculate the equation of state and elastic constants of simple metals and ordered binary intermetallic alloys. In most cases the equilibrium lattice constants are underestimated by 1–2%, which is typical of other LDA calculations. A small portion of this error represents the error in neglecting zero-point motion and thermal expansion, and the remaining error is from the LDA. We have also shown that we can successfully predict the elastic constants of these materials, typically to within 10% of experiment, with a maximum error of about 20%. These elastic constants can be used to estimate the shear modulus in polycrystalline materials, where we again successfully compared our results with experiment. Finally, we showed that the elastic constants are roughly correlated with the melting temperature of the solid.

What is the future of first-principles calculations? In addition to 'predicting' the melting temperature using (39) and (40), we have also looked at the barriers that prevent the lattice from 'hopping' between various phases with the same structure but different orientations. There is some indication that this 'magic strain barrier height' is correlated to the melting temperature (Mehl and Boyer, 1991). Simple models of defects have also been studied. In particular, first-principles calculations have been used to determine the vacancy formation

energy in aluminum (Dentenerr and Soler, 1991; Mehl and Klein, 1991; Benedek *et al.*, 1992). This number is important for studying defects in solids and the motion of dislocations, which can be pinned by defects. The first-principles calculations required to do further work in this area are rather complex and computer-intensive, but are within the range of calculations that can be handled by the current generation of workstation computers.

Computer limitations inhibit the use of first-principles calculations to study large systems (thousands of atoms) using the DFT but, as the work of Rifkin *et al.* (1992) indicates, such calculations can be used to fit model many-body potentials for materials that do not exist in Nature or whose experimental parameters are difficult to obtain. These potentials can then be used to predict the behavior of large numbers of atoms, including defect energies, dislocations and their motion, and interface effects. Although the current generation of first-principles algorithms cannot handle these problems, the new generation of parallel computers and new algorithms that are being developed (Baroni and Giannozzi, 1992; Galli and Parrinello, 1992) indicate that in the future we may be able to handle these systems more accurately.

6. Acknowledgements

This work was partially supported by the Office of Naval Research, US Department of Defense. Thanks are due to S. Chubb, who did the initial calculations for the TiAl system, J. E. Osburn, who helped with the remaining calculations, and H. Krakauer, S. Wei and D. Singh for the constantly improving full-potential LAPW code.

7. Appendix

7.1 Determination of Errors in the Elastic Moduli

As noted in the discussion in Section 3.1, the numerical noise in the total-energy calculations sometimes makes it difficult to determine the proper order N we should take for the Birch expansion (17), and to determine the possible range in values for the parameters E_0, V_0, B_0, and B_0'. A similar problem arises in Section 3.2, where we wish to fit our data to a polynomial in x^2 and to estimate the errors in the corresponding elastic constant. In this appendix we outline the procedure we use in fitting the Birch equation (17). The procedure for fitting the elastic constants is similar, and simpler, because we are only interested in the error bars in one quantity, the appropriate linear combination of the C_{ij}.

In fitting (17), we are given a set of volume–energy points, (V_i, E_i). To determine the best point N to choose for a given set of data, we follow a procedure outlined in Press *et al.* (1986). We first estimate the error for each E_i. In these calculations we do this by computing E_i for several **k**-point meshes, average the energy weighted by the number of **k** points in each mesh, and use the similarly weighted standard deviation, σ_i, as the error estimate. We then choose the parameters in (17) to minimize the quantity

$$\chi^2 = \sum_{i=1}^{M} [E_i - E_B(V_i)]^2/\sigma_i^2 \qquad \text{(A1)}$$

where M is the number of (V_i, E_i) pairs. Assuming the errors are normally distributed, the probability that inserting another set of energies E_i (perhaps calculated in a slightly different manner, or from a different starting density) and the just calculated parameters E_0, V_0, B_0, B_0', and γ_n into (A1) will produce an error no worse than χ^2 is given by

$$q = \int_{\chi^2/2}^{\infty} t^{(M-N-3)/2} e^{-t} dt/\Gamma((M-N-1)/2) \qquad \text{(A2)}$$

We therefore choose the value N that gives the largest value of q. For a good fit q will be on the order of 0.1. If our estimated σ_i are too large, as sometimes happens with the **k**-point averaging method, then q will be around 0.9. Of course, it is likely that some of the errors in our calculations are systematic instead of normally distributed, in which case the value of q is not quite accurate, but this procedure gives a convenient way of choosing the cutoff N.

We can also estimate the errors in the equilibrium parameters. As an example, consider the equilibrium bulk modulus B_0. We can refit the Birch equation (17) by freezing the 'equilibrium' modulus at some value β_0 and then let all of the other parameters change to minimize the new error $\chi^2(\beta_0) > \chi^2(B_0)$. If the errors in our calculation are normally distributed, then there is a 68.3% probability that the true equilibrium modulus is within the range of β_0 values that satisfy the condition

$$\chi^2(\beta_0) < \chi^2(B_0) + 2.3 \qquad \text{(A3)}$$

The error bars on B_0 quoted in Tables 2 and 4 show the range of β_0 values that satisfy (A3). The procedures for the other parameters of (17) and the elastic constants in Section 3.2 follow the same rules.

7.2 Polycrystalline Bounds on the Bulk and Shear Moduli

As we noted in Section 3.2, our calculated single-crystal elastic constants can be used to compute bounds on the bulk and shear moduli observed in isotropic polycrystalline samples of the material. We use this appendix to list the equations that construct these bounds.

For cubic systems the results are rather simple. The isotropic bulk modulus B is given exactly by (25). The shear modulus, which would obey the relationship (Schreiber *et al.*, 1973) $G^{\mathrm{I}} = C^{\mathrm{I}}_{44} = (C^{\mathrm{I}}_{11} - C^{\mathrm{I}}_{12})/2$ in an isotropic solid, is bounded from below by the Reuss (1929) modulus G_{R}, and from above by the Voigt (1928) modulus G_{V}:

$$\begin{aligned} &G_{\mathrm{R}} < G < G_{\mathrm{V}} \\ &G_{\mathrm{R}} = 5(C_{11} - C_{12})C_{44}/[4C_{44} + 3(C_{11} - C_{12})] \\ &G_{\mathrm{V}} = (C_{11} - C_{12} + 3C_{44})/5 \end{aligned} \tag{A4}$$

There are analogous, although more complicated, expressions for the tetragonal lattice. The isotropic bulk modulus B is bounded by:

$$\begin{aligned} &B_{\mathrm{R}} < B < B_{\mathrm{V}} \\ &B_{\mathrm{R}} = [(C_{11} + C_{12})C_{33} - 2C_{13}^2]/(C_{11} + C_{12} + 2C_{33} - 4C_{13}) \\ &B_{\mathrm{V}} = (2C_{11} + C_{33} + 2C_{12} + 4C_{13})/9 \end{aligned} \tag{A5}$$

Note that B_{R} has exactly the form (26). The bounds on the shear modulus are given by:

$$\begin{aligned} G_{\mathrm{R}} = 15C(C_{11} - C_{12})C_{44}C_{66}/\{2(C_{11} - C_{12})[2(C_{11} + C_{12}) + 4C_{13} + C_{33}]C_{44}C_{66} + \\ 3C[2C_{44}C_{66} + (C_{11} - C_{12})(C_{44} + 2C_{66})]\} \\ G_{\mathrm{V}} = (2C_{11} + C_{33} - C_{12} - 2C_{13} + 6C_{44} + 3C_{66})/15 \end{aligned} \tag{A6}$$

where

$$C = C_{33}(C_{11} + C_{12}) - 2C_{13}^2 \tag{A7}$$

For the cubic case, stricter bounds were derived by Hashin and Shtrikman (1962). The bulk modulus B is given by (25), as before. However, the shear modulus G is bounded by

$$\begin{aligned} G_1 &= G_1^* + 3/[5/(G_2^* - G_1^*) - 4\beta_1] \\ G_2 &= G_2^* + 2/[5/(G_1^* - G_2^*) - 6\beta_2] \end{aligned} \tag{A8}$$

where

$$G_1^* = (C_{11} - C_{12})/2 \qquad G_2^* = C_{44} \tag{A9}$$

and

$$\begin{aligned} \beta_1 &= -3(B + 2G_1^*)/[5G_1^*(3B + 4G_1^*)] \\ \beta_2 &= -3(B + 2G_2^*)/[5G_2^*(3B + 4G_2^*)] \end{aligned} \tag{A10}$$

We will use the term Hashin modulus (G_{H}) for the larger of G_1 and G_2, and the Shtrikman modulus (G_{S}) for the smaller. The shear modulus G in cubic systems is thus bounded by

$$G_{\mathrm{S}} < G < G_{\mathrm{H}} \tag{A11}$$

One should note that in cubic systems the range of the bounds $G_{\mathrm{V}} - G_{\mathrm{R}}$ or $G_{\mathrm{H}} - G_{\mathrm{S}}$ depends upon the anisotropy parameter A (35). When $A = 1$ the system is isotropic, the bounds vanish, and G is given by either of the relationships in equation (A9).

8. References

Andersen, O. K. (1975). *Phys. Rev.*, **B12**, 3060.

Ashcroft, N. W., and Mermin, N. D. (1976). *Solid State Physics*. Holt, Reinhart and Winston, New York.

Baroni, S., and Giannozzi, P. (1992). *Europhys. Lett.*, **17**, 547.

Becquart, C. (1992). Ph.D. Thesis, University of Connecticut.

Benedek, R., Yang, L. H., Woodward, C., and Yin, B. I. (1992). *Phys. Rev.*, **B45**, 2607.

Birch, F. (1978). *J. Geophys. Res.*, **83**, 1257.

Boyer, L. L. (1989). *Acta Crystallogr.*, **A45**, FC29.

Boyer, L. L., Kaxiras, E., Feldman, J. L., Broughton, J. Q., and Mehl, M. J. (1991). *Phys. Rev. Lett.*, **67**, 715.

Chen, J., Boyer, L. L., Krakauer, H., and Mehl, M. J. (1988). *Phys. Rev.*, **B37**, 3295.

Chubb, S. R., Papaconstantopoulos, D. A., and Klein, B. M. (1988). *Phys. Rev.*, **B38**, 12120.

Dentenerr, P. J. H., and Soler, J. M. (1991). *Solid State Commun.*, **78**, 857.

Donohue, J. *The Structure of the Elements*. Wiley, New York.

Featherstone, F. H., and Neighbors, J. R. (1963). *Phys. Rev.*, **130**, 1324.

Feldman, J. L., Mehl, M. J., and Krakauer, H. (1987). *Phys. Rev.*, **B35**, 6375.

Feldman, J. L., Mehl, M. J., Boyer, L. L., and Chen, C. (1988). *Phys. Rev.*, **B37**, 4784.

Fine, M. E., Brown, L. D., and Marcus, H. L. (1984). *Scr. Metall.*, **18**, 951.

Fleischer, R. L. (1991a). In *Intermetallic Compounds* (ed. O Izumi). Japan Institute of Metals, Sendai, p. 157.

Fleischer, R. L. (1991b). *ISIJ Int.*, **31**, 1186.

Fleischer, R. L. (1993a). *J. Mater Res.*, **7**, 49.
Fleischer, R. L. (1993b). *Acta Metall. Mater.*, **41**, 863; (1992). General Electric Report 92CRD 214.
Fleischer, R. L., Gilmore, R. S., and Zabala, R. J. (1989). *Acta Metall.*, **37**, 2801.
Galli, G., and Parrinello, M. (1992). *Phys. Rev. Lett.*, **69**, 3547.
Gilmore, R. S. (1968). PhD thesis, Rensselaer Polytechnic Institute, Troy, NY.
Hashin, Z., and Shtrikman, S. (1962). *J. Mech. Phys. Solids*, **10**, 335, 343.
Hedin, L., and Lundqvist, B. I. (1971). *J. Phys.*, **C4**, 2064.
Hohenberg, P., and Kohn, W. (1964). *Phys. Rev.*, **136**, B864.
Johnson, D. D. (1988). *Phys. Rev.*, **B38**, 12807.
Kittel, C. (1986). *Introduction to Solid State Physics*, 6th Edn. Wiley, New York.
Koelling, D. D., and Arbman, G. O. (1975). *J. Phys.*, F5, 2041.
Koelling, D. D., and Harmon, B. N. (1977). *J. Phys.*, C10, 3107.
Kohn, W., and Sham, L. J. (1965). *Phys. Rev.*, **140**, A1133.
Massalski, T. B., Murray, J. L., Bennett, L. H., and Baker, H. (eds) (1986). *Binary Phase Diagrams*. American Society for Metals, Metals Park, OH.
Mehl, M. J., and Boyer, L. L. (1991). *Phys. Rev.*, **B43**, 9498.
Mehl, M. J., and Klein, B. M. (1991). *Physica*, **B172**, 211.
Mehl, M. J., and Pickett, W. E. (1989). In *Raman Scattering, Luminescence, and Spectroscopic Instrumentation in Technology*. SPIE 1055, p. 191.
Mehl, M. J., Cohen, R. E., and Krakauer, H. (1988). *J. Geophys. Res.*, **93**, 8009; (erratum). (1989). *J. Geophys. Res.*, **94**, 1977.
Mehl, M. J., Osburn, J. E., Papaconstantopoulos, D. A., and Klein, B. M. (1990). *Phys. Rev.*, **B41**, 10311; (erratum). (1991). *Phys. Rev.*, **B42**, 5362.
Mehl, M. J., Osburn, J. E., Papaconstantopoulos, D. A., and Klein, B. M. (1991). *Mater. Res. Soc. Symp. Proc.*, 186, 227.
Monkhorst, H. J., and Pack, J. D. (1976). *Phys. Rev.*, B13, 5188.
Moroni, E. G. (1992). PhD thesis, Université de Lausanne, Switzerland, unpublished.
Moruzzi, V. L., Janak, J. F., and Williams, A. R. (1978). *Calculated Electronic Properties of Metals*. Pergamon, New York.
Moruzzi, V. L., Janak, J. F., and Schwarz, K. (1988). *Phys. Rev.*, **B37**, 790.
Osburn, J. E., Mehl, M. J., and Klein, B. M. (1991). *Phys. Rev.*, **B43**, 1805.
Papaconstantopoulos, D. A., and Singh, D. (1990). *Phys. Rev.*, **B45**, 7507.
Pearson, W. B. (1967). *A Handbook of Lattice Spacings and Structures of Metals and Alloys*, Vol. 2. Pergamon, Oxford.
Perdew, J. P., Chevary, J. A., Vosko, S. H., Jackson, K. A., Pederson, M. R., Singh, D. J., and Fiolhais, C. (1992). *Phys. Rev.*, **B46**, 6671.
Pickett, W. E. (1985). *Solid State Phys.*, **12**, 1.
Pickett, W. E., and Wang, C. S. (1984). *Phys. Rev.*, **B30**, 4719.
Press, W. H., Flannery, B. P., Teukolsky, S. A., and Vetterling, W. T. (1986). *Numerical Recipes: The Art of Scientific Computing*. Cambridge University Press, Cambridge.
Reuss, A. (1929). *Z. Angew, Math. Mech.*, **9**, 49.
Rifkin, J. A., Becquart, C. S., Kim, D., and Clapp, P. (1992). *Mater. Res. Soc. Proc.*, **278**, 173.
Schreiber, E., Anderson, O. L., and Soga, N. (1973). *Elastic Constants and Their Measurement*. McGraw-Hill, New York.
Siglas, M., Bacalis, N. C., Papaconstantopoulos, D. A., Mehl, M. J., and Switendick, A. C. (1990). *Phys. Rev.*, **B42**, 11637.
Sigalas, M., Papaconstantopoulos, D. A., and Bacalis, N. C. (1992). *Phys. Rev.*, **B45**, 5777.
Simmons, G., and Wang, H. (1971). *Single Crystal Elastic Constants and Calculated Aggregate Properties: A Handbook*, 2nd Edn. MIT Press, Cambridge, MA.
Singh, D. (1991). *Phys. Rev.*, **B43**, 6388.
Singh, D., and Papaconstantopoulos, D. A. (1990). *Phys. Rev.*, **B49**, 8885.
Singh, D., Krakauer, H., and Wang, C. S. (1986). *Phys. Rev.*, **B34**, 8391.
Terakura, K., Williams, A. R., Oguchi, T., and Kübler, J. (1984). *Phys. Rev. Lett.*, **52**, 1830.
Van de Waal, B. W. (1990). *Acta Crystallogr.*, **A46**, FC17.
Voigt, W. (1928). *Lehrbuch der Kristallphysik*. Teubner, Leipzig.
Wallow, F., Neite, G., Schröer, W., and Nembach, E. (1987). *Phys. Status Solidi*, **A99**, 483.
Wei, S. H., and Krakauer, H. (1985). *Phys. Rev. Lett.*, **55**, 1200.
Wills, J. M., Eriksson, O., Söderland, P., and Boring, A. M. (1992). *Phys. Rev. Lett.*, **68**, 2802.